JOURNAL OF SOLID STATE CHEMISTRY 96, 397–407 (1992)

Structure and Phase Transition in the Spinel System $Li_{1-x}CuVO_4$ ($0 \leq x \leq 0.2$), with One-Dimensional Cooperative Jahn–Teller Ordering

R. KANNO* AND Y. KAWAMOTO

Department of Chemistry, Faculty of Science, Kobe University, Kobe 657, Japan

Y. TAKEDA, M. HASEGAWA,† AND O. YAMAMOTO

Department of Chemistry, Faculty of Engineering, Mie University, Tsu 514, Japan

AND N. KINOMURA

Institute of Inorganic Synthesis, Yamanashi University, Miyamae-cho 7, Kofu 400, Japan

Received November 14, 1990; in revised form July 29, 1991

Structure and phase transition in the spinel $Li_{1-x}CuVO_4$ were characterized by X-ray Rietveld structure refinement, magnetic susceptibility, high-temperature X-ray diffraction, and differential scanning calorimetry measurements. The nonstoichiometric $Li_{1-x}CuVO_4$ was synthesized in the range of $0 \leq x \leq 0.2$. In the structure of $Li_{1-x}CuVO_4$, the $[CuO_6]$ octahedra are connected to each other one-dimensionally parallel to the a axis, such that the elongated octahedral axis is ordered along the c axis. A low-temperature modification of $Li_{1-x}CuVO_4$ prepared by annealing the sample at 80°C showed a phase transition near 100°C. The high-temperature phase was also quenched to ambient temperature. The Jahn–Teller distortion of the $[CuO_6]$ octahedra decreased with the increase in the non-Jahn–Teller Cu^{3+} ions for the low-temperature $Li_{1-x}CuVO_4$. Further, one- and two-dimensional cooperative ordering crystal structures have been discussed.

Introduction

Jahn–Teller distortions in the spinel structure have been widely studied from the viewpoint of the arrangement in a lattice of the orbital directions of certain anisotropic ions. In the ideal cubic AB_2O_4 spinel structure the oxygen ions form a cubic close packed lattice with the A and B cations occupying, respectively, $\frac{1}{8}$ of the tetrahedrally and $\frac{1}{2}$ of the octahedrally coordinated interstices. The large tetragonal distortion which occurs in a number of spinels such as $ZnMn_2O_4$, $MgMn_2O_4$, $CuFe_2O_4$, and $CuCr_2O_4$ arises as a consequence of a Jahn–Teller type distortion in the immediate environment of ions with d^4, d^9 in a high spin state (*1–3*).

*To whom correspondence should be addressed.

†Present address: Living System Research Center, Matsushita Electric Industrial Co., Ltd., Moriguchi, Osaka 570, Japan.

0022-4596/92 $3.00

The cooperative Jahn–Teller effect has also been observed as a consequence of higher concentrations of Jahn–Teller ions in the octahedra which are either isolated from each other or connected in one, two, or three dimensions via common corners, edges, or faces. One dimensional cooperative ordering has been found, for example, in A_2MnF_5 (A = Rb, Cs, NH_4) (*4, 5*), Na_2MX_4 (M = Cr, Cu; X = F, Cl) (*6, 7*) and ABX_3 (A = Rb, Cs; B = Cr, Cu; X = Cl, Br, I) compounds (*8–12*).

We have recently found a new example of one dimensional cooperative ordering in Li_2CrCl_4 with the spinel structure (*13*). Li_2CrCl_4 was derived from the cubic inverse spinel structure where half of the lithium ions together with the chromium ions are situated on the octahedral sites. The lattice distortion from cubic symmetry was caused by a 1 : 1 ordering on the octahedral sites such that the lithium ions and the chromium ions ordered one dimensionally. For oxide spinels, one dimensional ordering of the Jahn–Teller ion has been previously reported for $LiCuVO_4$ (*14, 15*). The lithium and the copper ions in $LiCuVO_4$ are situated on the octahedral sites and the vanadium ions on the tetrahedral sites. The orthorhombic distortion is caused by the one dimensional ordering of the lithium and the copper ions.

The room temperature monoclinic phase of Li_2CrCl_4 transforms to a cubic phase with a random cationic arrangement on the octahedral sites through the two-phase region. On the other hand, $LiCuVO_4$ shows no phase transition up to its melting. The extent of the Jahn–Teller deformation of the single $[CuO_6]$ polyhedra might decrease with decreasing Cu^{2+} concentration, and further, might affect a phase transition driven by either static or dynamic cooperative coupling. In this paper, we report how the decrease in the Jahn–Teller ions affects the lattice distortion of the spinel structure with a one dimensional cooperative ordering system. The Jahn–Teller ordering behavior in $LiCuVO_4$ was examined by substituting Cu^{2+} into Cu^{3+} ions. As a result, the solid solution $Li_{1-x}CuVO_4$ was synthesized, and the phase transition from a low-temperature to a high-temperature modification was found. Further, one and two dimensional cooperative ordering crystal structures have been discussed.

Experimental

Copper oxide, Lithium Carbonate and vanadium pentaoxide were used: CuO, $LiCO_3$, V_2O_5 (Nakarai Co., >99% purity). The appropriate quantities of reactants were ground together, pressed into a pellet at 60 MPa, and heated in air at 530°C for 1 week. X-ray diffraction (XRD) patterns of the powdered samples were obtained using monochromated Cu$K\alpha$ radiation and a scintillation detector.

XRD data for Rietveld analysis were collected on the polycrystalline samples using a high power X-ray powder diffractometer (Rigaku RAD-RC 12kW). The focusing graphite monochromator equipped after the sample was used for employing Cu$K\alpha$ radiation. Diffraction data were collected for 2 sec at each 0.02° step width over a 2θ range from 15° to 105° at room temperature. Structural refinement of the XRD data was performed using the Rietveld analysis computer program RIETAN provided by Izumi (*16*). Reflection positions and intensities were calculated for both Cu$K\alpha_1$ (λ = 1.5405 Å) and Cu$K\alpha_2$ (λ = 1.5443 Å) with a factor of 0.5 applied to the latter's calculated integrated intensities. A pseudo-Voigt profile function was used; the mixing parameter γ was included in the least-squares refinement.

The high-temperature phases were examined with a high-temperature X-ray diffractometer with monochromated Cu$K\alpha$ radiation. Differential scanning calorimetry (DSC) was carried out between 77 and 773

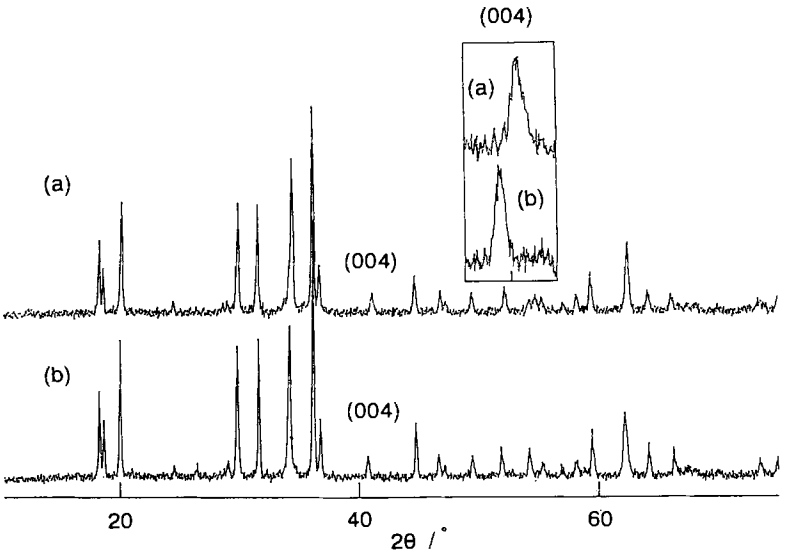

FIG. 1. X-ray diffraction patterns for $Li_{0.8}CuVO_4$ of (a) low-temperature modification and (b) high-temperature modification.

K for samples sealed in alumina containers with α-Al_2O_3 as a standard. Heating and cooling rates were 10 K/min. The latent heat ΔH for a transition was calculated from ΔH_{melt} of Sn and In metal as a standard. Magnetic susceptibility was measured using a Faraday balance from 77 to about 450 K.

Results

The solid solution $Li_{1-x}CuVO_4$ synthesized at 530°C showed XRD patterns similar to those of the stoichiometric $LiCuVO_4$. However, the (004) line was split into doublet when the samples were cooled slowly from 530°C. This splitting might be caused by the following reasons: (i) a low-temperature modification was formed by the slow cooling process and this phase had a lower symmetry than a high-temperature modification; (ii) the samples cooled slowly from 530°C were a mixture of a low-temperature modification and a high-temperature modification, each phase has a different c parameter. It was therefore expected that the annealing just below the transition temperature would facilitate equilibrium and enable the monophasic low-temperature modification to be obtained. DSC measurements of the samples cooled slowly from 530°C showed a broad endothermic peak around 100°C; the annealing at 80°C for 1 week was examined. The XRD patterns of the samples thus obtained indicated no (004) line splittings and, in addition, no extra reflections due to a superlattice or a symmetry reduction from space group *Imma*. The monophasic low-temperature phase was therefore obtained by annealing it at 80°C and that the samples cooled slowly from 530°C were a mixture of the low-temperature and the high-temperature modifications of $Li_{1-x}CuVO_4$. Further, the monophasic high-temperature modification was obtained by quenching it into liquid nitrogen from 530°C. Figure 1 shows the XRD patterns of the high-temperature and the low-temperature $Li_{0.8}CuVO_4$. The XRD patterns are quite similar to each other, except for the position of the (004) lines.

Figure 2 shows the lattice parameter changes for the high-temperature and the

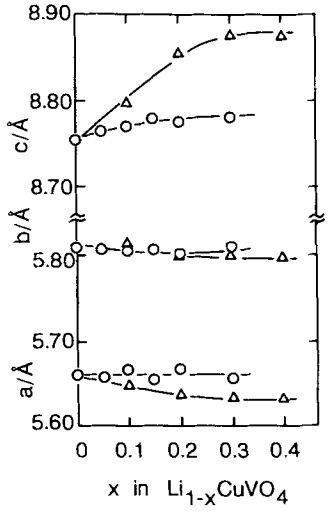

FIG. 2. Composition dependence of the lattice parameters for high-temperature $Li_{1-x}CuVO_4$ (△) and low-temperature $Li_{1-x}CuVO_4$ (○).

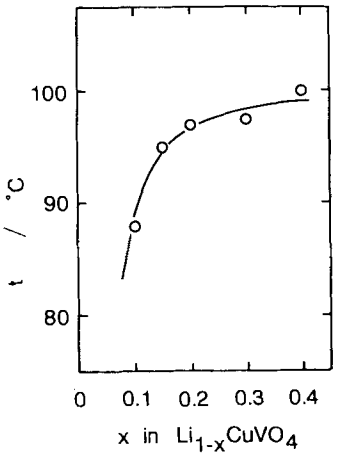

FIG. 3. Composition dependence of the transition temperature of $Li_{1-x}CuVO_4$.

low-temperature $Li_{1-x}CuVO_4$. The c parameters of the high-temperature phases increase from 8.75 to 8.88 Å with x ranging from $x = 0.0$ to 0.3, while for the a and b axes, slight decreases in the parameters are observed from $x = 0.0$ to 0.3. The c parameters of the low-temperature phases increase from 8.75 to 8.78 Å with increasing x from 0.0 to 0.3, and no significant changes were found in the a and b parameters. Extra XRD peaks due to impurities were observed for the samples with $x \geq 0.3$ in both the high-temperature and low-temperature phases. The compositional range of the solid solution was therefore determined to be $0.0 \leq x \leq 0.2$.

The amounts of lithium, copper, and vanadium ions in the nonstoichiometric $Li_{0.8}CuVO_4$ were determined by emission spectrography. The Li : Cu : V ratio determined to be 0.79 : 1.0 : 1.0 was consistent with the composition of the raw material, indicating that loss of lithium during the sample preparation was negligibly small.

DSC measurements were carried out for the samples annealed at 80°C in order to confirm the phase transition. The endothermic peaks were clearly observed around 150°C on heating. Figures 3 and 4 show respectively the composition dependence of the transition temperature and the composition dependence of the latent heat for the transition. The transition temperature increases from 88°C at $x = 0.1$ to 97°C at $x = 0.2$, and the latent heat increases from 1.0

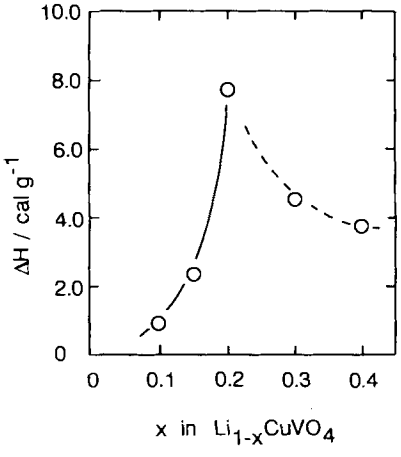

FIG. 4. Latent heat ΔH as a function of x in $Li_{1-x}CuVO_4$.

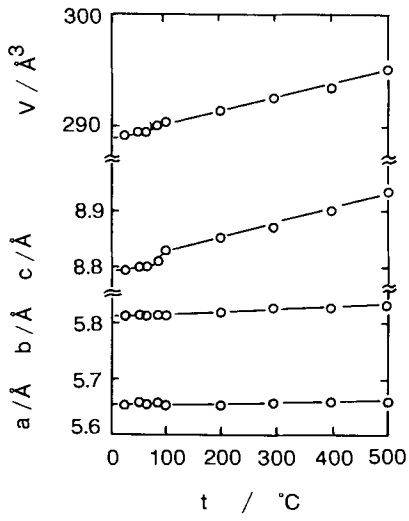

FIG. 5. Thermal evolution of lattice parameters for $Li_{0.8}CuVO_4$.

cal g^{-1} at $x = 0.1$ to 7.7 cal g^{-1} at $x = 0.2$. The transition was also confirmed by the high-temperature XRD measurements for $Li_{0.8}CuVO_4$. Figure 5 shows thermal evolution of the lattice parameters for $Li_{0.8}CuVO_4$ annealed at 80°C. The curves showed a change in slope at 100°C, being consistent with the transition at 97°C indicated by the DSC measurements. Magnetic susceptibilities were measured for $Li_{0.9}CuVO_4$ (HT) and $Li_{0.9}CuVO_4$ (LT). The susceptibilities are well described by the Curie–Weiss law. The magnetic moments are calculated respectively to be 2.05 BM with the paramagnetic Curie temperature $\theta_c = -39.0$ K, and 2.01 BM with $\theta_c = 32.4$ K, for $Li_{0.9}CuVO_4$ (HT) and $Li_{0.9}CuVO_4$ (LT).

The structure of $Li_{1-x}CuVO_4$ was determined by X-ray Rietveld method in order to clarify the ligand environment of Cu^{2+} ions. Refinements were carried out for $LiCuVO_4$, the high-temperature $Li_{1-x}CuVO_4$ ($x = 0.1$, 0.2), and the low-temperature $Li_{1-x}CuVO_4$ ($x = 0.1$, 0.2). Initial coordinates for the model were those reported for $LiCuVO_4$ with space group *Imma*. Refinement proceeded smoothly to yield agreement factors $R_{wp} = 4.19\%$, $R_p = 2.86\%$, and $R_I = 3.59\%$, with expected agreement $R_E = 2.23\%$ for $LiCuVO_4$. For the low-temperature $Li_{0.8}CuVO_4$, initial refinement using the above positional parameters proceeded to agreement factors, $R_{wp} = 3.64\%$, $R_p = 2.76\%$, and $R_I = 4.27\%$ with negative B values on 4*e* and 4*d* sites. We thus repeated the refinement with an extra condition, taking into account a partial disorder of the Cu^{2+} ions on the 4*a* and 4*d* sites. The occupancies on 4*e* and 4*d* sites were refined using the constraints that the total composition of Cu^{2+} ions was 0.8. Refinement proceeded to the agreement factors $R_{wp} = 3.55\%$, $R_p = 2.68\%$, and $R_I = 3.65\%$ with expected agreement $R_E = 1.90\%$. The partial disorder of the Cu^{2+} ions was taken into account for all nonstoichiometric $Li_{1-x}CuVO_4$ systems. Preferred orientation parameters were also taken into account for the high-temperature $Li_{0.8}CuVO_4$ phase. Refinement results are summarized in Table I. Observed, calculated, and difference plots of $Li_{0.9}CuVO_4$ (HT) are shown in Fig. 6. Table II lists the interatomic distances and bond angles.

Discussion

(*a*) *Jahn–Teller Crystallography of* $Li_{1-x}CuVO_4$

The structure refinement results for $LiCuVO_4$ are well consistent with those reported by Durif *et al.* (*15*). The distortion of the $[CuO_6]$ octahedra is appreciably large (Cu–O(1): 2.436(10) Å (×2); Cu–O(2): 1.954(7) Å (×4)). The $[CuO_6]$ octahedra are connected to each other one dimensionally parallel to the *a* axis by sharing O(2)–O(2) edges, such that the elongated octahedral axis ordered in the same direction parallel to the *c* axis. Figure 7 shows the bond distances in $Li_{1-x}CuVO_4$ as a function of x. For the low-temperature modification, the Cu–O(1) distances decrease with x. The introduction of the non-Jahn–Teller Cu^{3+} ions

TABLE 1

RIETVELD REFINEMENT RESULTS FOR $Li_{1-x}CuVO_4$

	$LiCuVO_4$	$Li_{0.9}CuVO_4$ LT	$Li_{0.9}CuVO_4$ HT	$Li_{0.8}CuVO_4$ LT	$Li_{0.8}CuVO_4$ HT
Scale factor	0.02404(1)	0.03958(2)	0.04484(2)	0.02775(1)	0.04972(4)
FWHM parameter U	0.10(1)	0.36(2)	0.15(1)	0.16(2)	0.46(2)
V	−0.050(9)	−0.266(1)	−0.090(8)	−0.070(1)	−0.233(1)
W	0.034(2)	0.086(3)	0.039(1)	0.023(3)	0.058(3)
Asymmetry parameter	0.37(3)	0.78(3)	0.71(4)	0.42(2)	0.52(3)
Gaussian fraction	0.21(1)	0.30(1)	0.27(1)	0.14(3)	0.25(1)
FWHM (Gauss)/ FWHM (Lorentz)	1.41(6)	1.52(4)	1.54(4)	0.84(7)	1.61(5)
Preferred-orientation 1	—	—	—	—	0.75(1)
parameter 2	—	—	—	—	1.3(1)
Lattice constants a(Å)	5.6517(1)	5.6482(1)	5.6435(1)	5.6492(1)	5.6377(1)
b	5.7987(1)	5.7981(1)	5.7983(1)	5.7988(1)	5.7941(1)
c	8.7476(2)	8.7614(2)	8.7812(2)	8.7622(2)	8.8136(2)
R_{wp}	4.19	3.81	4.45	3.55	4.73
R_p	2.86	2.72	3.05	2.68	3.42
R_I	3.59	2.92	3.58	3.65	4.50

Atom	Site	Occupancy	Fractional coordinates x	y	z	B(Å^2)
		Rietveld refinement results for $LiCuVO_4$				
V	4*e*	1	0.0	0.25	0.3865(6)	0.2(1)
Cu	4*a*	1	0.0	0.0	0.0	0.6(1)
Li	4*d*	1	0.25	0.25	0.75	0.1(1)
O(1)	8*h*	1	0.0	0.014(2)	0.278(1)	0.1(2)
O(2)	8*i*	1	0.231(1)	0.25	−0.001(1)	0.1(2)
		Rietveld refinement results for $Li_{0.9}CuVO_4$(LT)				
V	4*e*	1	0.0	0.25	0.3852(7)	0.2(2)
Cu	4*a*	0.954(6)	0.0	0.0	0.0	0.8(1)
Li	4*d*	0.9	0.25	0.25	0.75	0.8
Cu	4*d*	0.045(6)	0.25	0.25	0.75	0.8
O(1)	8*h*	1	0.0	0.020(2)	0.276(1)	1.4(4)
O(2)	8*i*	1	0.240(1)	0.25	0.000(2)	1.3(4)
		Rietveld refinement results for $Li_{0.9}CuVO_4$(HT)				
V	4*e*	1	0.0	0.25	0.3862(8)	0.5(2)
Cu	4*a*	0.954(6)	0.0	0.0	0.0	1.5(2)
Li	4*d*	0.9	0.25	0.25	0.75	1.5
Cu	4*d*	0.045(6)	0.25	0.25	0.75	1.5
O(1)	8*h*	1	0.0	0.017(2)	0.277(1)	1.6(2)
O(2)	8*i*	1	0.234(1)	0.25	0.003(1)	0.9(4)
		Rietveld refinement results for $Li_{0.8}CuVO_4$ (LT)				
V	4*e*	1	0.0	0.25	0.3871(8)	0.2(2)
Cu	4*a*	0.963(7)	0.0	0.0	0.0	1.5(2)
Li	4*d*	0.8	0.25	0.25	0.75	1.5
Cu	4*d*	0.036(2)	0.25	0.25	0.75	1.5
O(1)	8*h*	1	0.0	0.024(2)	0.273(1)	1.5(4)
O(2)	8*i*	1	0.238(1)	0.25	0.001(1)	0.5(4)
		Rietveld refinement results for $Li_{0.8}CuVO_4$(HT)				
V	4*e*	1	0.0	0.25	0.3869(10)	0.5(2)
Cu	4*a*	0.946(8)	0.0	0.0	0.0	1.8(3)
Li	4*d*	0.8	0.25	0.25	0.75	1.8
Ci	4*d*	0.053(8)	0.25	0.25	0.75	1.8
O(1)	8*h*	1	0.0	0.020(2)	0.279(1)	1.1(4)
O(2)	8*i*	1	0.234(1)	0.25	0.005(1)	1.1

Note. LT = Low-temperature phase, HT = High-temperature phase.

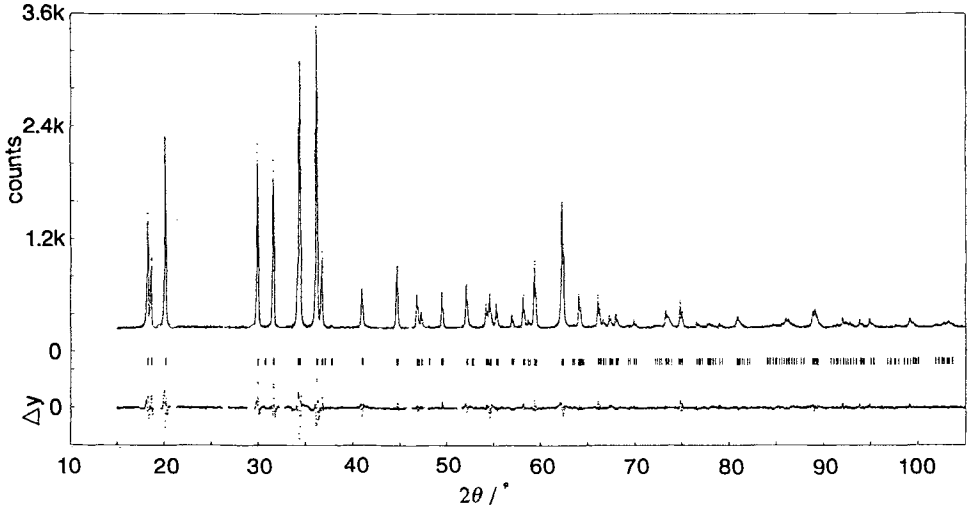

FIG. 6. Observed, calculated, and difference plots of $Li_{0.9}CuVO_4$ (HT) X-ray data.

in the 4*a* sites reduces the Cu–O(1) distances, which are the elongated axis of $[CuO_6]$ octahedra. On the contrary, the Li–O(1) and Li–O(2) distances in the $[LiO_6]$ octahedra increase with x. The structure refinements showed that the vacancies are located mainly on the lithium 4*d* sites; these vacancies lead to longer Li–O distances. The decrease in the c parameters with x, shown in Fig. 2, could be explained by the bond distance changes described above; introduction of the non-Jahn–Teller Cu^{3+} ions reduces the Cu–O(1) distances in the $[CuO_6]$ octahedra, and this variation exceeds the increase in the Li–O(2) distances caused by the vacancies.

The Jahn–Teller distortion is usually described by parameters which are directly calculated from the structural data. The radial (ρ) and angular (ψ) Jahn–Teller distortion parameters are defined by Ref. (*17*):

$$\rho = 2^{\frac{1}{2}}[(\Delta u)^2 + (\Delta v)^2 + (\Delta z)^2]^{\frac{1}{2}}$$

$$\mathrm{tg}\psi = 3^{\frac{1}{2}}\frac{\Delta u - \Delta v}{2\Delta z - \Delta u - \Delta v}.$$

From Table II, the following bond distances, for example, were derived for the low-temperature modification of $Li_{0.8}CuVO_4$:

in $[CuO_{4/2}]_\infty$ plane bond distances,

$$\bar{A} + \Delta u = 1.980 \text{ Å } (\times 2)$$

$$\bar{A} + \Delta v = 1.980 \text{ Å } (\times 2);$$

out of $[CuO_{4/2}]_\infty$ plane bond distances,

$$\bar{A} + \Delta z = 2.401 \text{ Å } (\times 2);$$

average Cu–O bond distance,

$$\bar{A} = 2.120 \text{ Å } (\times 6).$$

Since the structural results show a ferrodistortive ordering of tetragonally elongated $[CuO_6]$ octahedra with the long axis parallel to the c axis, the radial Jahn–Teller distortion parameter ρ is calculated for $Li_{1-x}CuVO_4$; the values thus obtained are plotted in Fig. 7 as a function of x. The ρ values decrease with x, indicating that the introduction of the non-Jahn–Teller Cu^{3+} ions in the Cu^{2+} sites reduces the Jahn–Teller distortion of $[CuO_6]$ octahedra.

In the high-temperature $Li_{1-x}CuVO_4$, the Cu–O(1) and Li–O(2) distances, which are parallel to the c axis, increase with x, while for the Cu–O(2) bonds, no distance changes

TABLE II

INTERATOMIC DISTANCES AND ANGLES FOR $Li_{1-x}CuVO_4$

Distance(Å) or angle(°)	Composition modification[a]				
	$LiCuVO_4$	$Li_{0.9}CuVO_4$ LT	$Li_{0.9}CuVO_4$ HT	$Li_{0.8}CuVO_4$ LT	$Li_{0.8}CuVO_4$ HT
			(CuO_6)octahedron		
Cu–Cu	2.8993	2.8990	2.8991	2.8994	2.8970
Cu–O(1) ×2	2.436(10)	2.421(10)	2.442(10)	2.401(11)	2.467(15)
Cu–O(2) ×4	1.954(7)	1.987(7)	1.987(7)	1.980(7)	1.961(8)
O(1)–Cu–O(2)	88.5(5)	88.1(4)	87.2(4)	87.1(4)	86.5(5)
O(2)–Cu–O(2)^{i}	84.2(3)	86.3(4)	84.8(4)	85.9(4)	84.7(5)
			(LiO_6)octahedron		
Li–Li	2.8258	2.8241	2.8217	2.8246	2.8188
Li–O(2)^{ii} ×2	2.183(14)	2.186(18)	2.229(14)	2.206(15)	2.253(17)
Li–O(1)^{iii} ×4	2.099(9)	2.121(10)	2.112(10)	2.135(10)	2.122(12)
O(2)^{ii}–Li–O(1)^{iii}	85.1(4)	84.7(3)	84.8(3)	85.5(3)	84.4(4)
O(1)^{iv}–Li–O(1)^{iii}	86.2(4)	84.8(4)	85.3(4)	83.8(4)	84.9(5)
			(VO_4)tetrahedron		
V–O(1) ×2	1.663(12)	1.641(13)	1.648(13)	1.645(13)	1.633(15)
V–O(2)^{ii} ×2	1.815(12)	1.780(13)	1.782(12)	1.766(12)	1.771(14)
O(1)–V–O(2)^{ii}	108.3(3)	108.3(3)	109.3(3)	109.4(3)	108.0(3)
O(1)–V–O(1)^{i}	110.6(6)	110.6(6)	108.6(8)	105.5(9)	109.2(12)

Note. The superscripts refer to atoms in the following positions:

(i) $-X, -Y + \frac{1}{2}, Z$ (iii) $-X, -Y, Z - 1$
(ii) $-X + \frac{1}{2}, -Y + \frac{1}{2}, -Z + \frac{1}{2}$ (iv) $X + \frac{1}{2}, -Y, Z + \frac{1}{2}$.

[a]LT = Low-temperature phase; HT = High-temperature phase.

were observed. Furthermore, the Jahn–Teller distortion parameter at $x = 0.2$ (ρ = 0.584 Å) is larger than that of the stoichiometric spinel (ρ = 0.555 Å). These structural changes, however, are inconsistent with those expected from the introduction of non-Jahn–Teller ions in the Cu^{2+} sites. The structure refinement results showed a larger copper ion occupancy on the 4*d* sites for the high-temperature $Li_{0.8}CuVO_4$ than for the low-temperature phase. The high-temperature phases might have a more disordered arrangement, such that a larger Jahn–Teller distortion of the CuO_6 octahedra is induced.

The DSC measurements on heating showed the endothermic peak around 150°C, while on cooling no exothermic peaks were observed. The sample preparation experiments also indicate that (i) the annealing below the transition temperature is necessary for the monophasic low-temperature modification to be obtained, and (ii) the high-temperature phases are easily quenched at room temperature. These results indicate that the transition from the low-temperature to the high-temperature phases proceeded much faster than that from the high-temperature phases. This transition could thus be considered as reorientation processes of cationic arrangements.

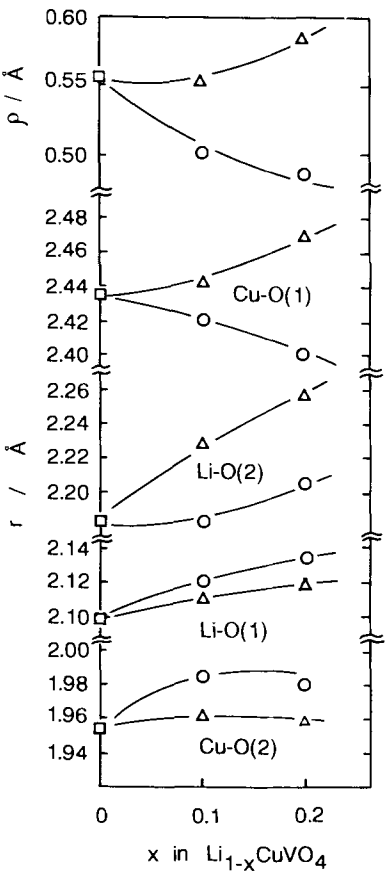

FIG. 7. Variation of bond distances and Jahn–Teller distortion parameter ρ as a function of x in $Li_{1-x}CuVO_4$ (△: high-temperature phase; ○: low-temperature phase).

(*b*) *One and Two Dimensional Cooperative Ordering Crystal Structures*

One and two dimensional cooperative ordering crystal structures have been previously reported in double halides and oxides. Table III lists examples of one and two dimensional cooperative ordering systems. Ions displaying the Jahn–Teller effect are normally coordinated octahedrally by anions. The octahedra are connected with each other by sharing faces, edges, and corners in one dimensional systems. The A_2MnF_5 compounds with A = Rb, Cs, NH_4exhibit infinite chains of the $Mn^{+3}F_6$ octahedra and sharing corners in *trans* configuration (*4, 5*). The Jahn–Teller effect of Mn^{+3} induces an axial distortion of the octahedra. Most $ACrX_3$ and $ACuX_3$ compounds (X = Cl, Br, or I; A = Rb or Cs) have $BaNiO_3$-type structures (*8–12*). In this structure, the $[BX_6]$ octahedra share faces forming infinite chains along the c axis. Several types of deformation with respect to the $BaNiO_3$ structure due to the cooperative Jahn–Teller effect have been reported.

One dimensional cooperative ordering in infinite chains connected by edge sharing octahedra have been found for Na_2CuF_4, Na_2CrF_4 (*6*), and Na_2CrCl_4 (*7*) with the Sr_2PbO_4-type structure and Li_2CrCl_4 (*13*) with the ordered spinel structure. Chains in the Sr_2PbO_4-type structure are formed by octahedra sharing opposite edges. Each divalent metal ion is surrounded by six Cl^- ions situated at the corners of a somewhat distorted octahedron. These octahedra share opposite edges to form infinite chains parallel to the a axis. The chains are held together by sodium ions; each sodium ion is surrounded by six Cl^- ions in trigonal prismatic coordination. The distortion of the

TABLE III

ONE-DIMENSIONAL AND TWO-DIMENSIONAL COOPERATIVE ORDERING CRYSTAL STRUCTURE

Sharing	Structure	Compound	Ref.
		One-dimensional ordering	
Corner	(A_2MnF_5)	Rb_2MnF_5, $(NH_4)_2MnF_5$	(*4*)
		Cs_2MnF_5	(*5*)
Edge	spinel	Li_2CrCl_4	(*13*)
		$LiCuVO_4$	this work
	Sr_2PbO_4	Na_2CuF_4, Na_2CrF_4	(*6*)
		Na_2CrCl_4	(*7*)
Face	$BaNiO_3$	Rb_2CuCl_4	(*8*)
		$CsCuCl_3$	(*9*)
		$RbCrCl_3$, $CsCrCl_3$	(*10, 11*)
		$RbCrI_3$, $CsCrI_3$	(*12*)
		Two-dimensional ordering	
		Rb_2CrCl_4	(*18, 19*)
Corner	K_2NiF_4	K_2CuF_4	(*20–22*)
		La_2CuO_4	(*23, 24*)
	$CsFeF_4$	$CsMnF_4$	(*25*)

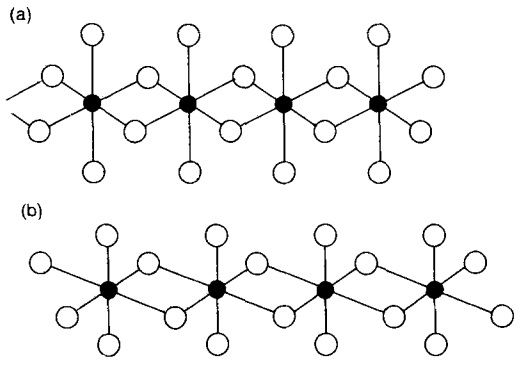

FIG. 8. Chain structure of (a) $LiCuVO_4$ and (b) Li_2CrCl_4.

$[CrCl_6]$ octahedra in Na_2CrCl_4 is appreciably large (Cr–Cl(2) : 2.463(×2) Å; Cr–Cl(2) : 2.902(×2) Å; Cr–Cl(1) : 2.431(×2) Å), while in isostructural Na_2MCl_4 (M = Mg, Mn, Cd), only a slight difference in M–Cl distance was observed (*7*). The $[CrCl_6]$ octahedra are connected to each other parallel to the a axis by sharing Cl(1)–Cl(1) edges, such that the elongated octahedral axis ordered in the same direction in the $[CrCl_{4/2}]_\infty$ plane (see Fig. 8).

The lithium chloride spinel, Li_2CrCl_4, with monoclinic symmetry, shows one dimensional cooperative ordering similar to that found in Na_2CrCl_4. The structure of Li_2CrCl_4 was derived from a cubic inverse spinel structure, where half of the lithium ions together with the metal divalent ions are situated on the octahedral sites (*13*). The $[CrCl_6]$ octahedra, connected one dimensionally to each other by sharing Cl–Cl edges, show appreciably large distortions (Cr–Cl : 2.47(×4); 2.78(×2) Å). Of the ordered spinels with a composition of Li_2MCl_4 (M = Cr, Co, Fe), the chromium spinel has monoclinic symmetry, while the cobalt and the iron spinels show orthorhombic symmetry, (*26, 27*). The one dimensional rows of $[CrCl_6]$ octahedra and $[LiCl_6]$ octahedra are in directions separated by 85.2°, leading to the monoclinic lattice distortion, while two rows in the orthorhombic Li_2MCl_4 (M = Fe, Co) are at a right angle to each other. In both the Sr_2PbO_4-type and the ordered spinel structures, the ordered octahedral elongation caused by the strong Jahn–Teller effect gives rise to a lattice deformation reducing the symmetry from orthorhombic to monoclinic. In the structure of $LiCuVO_4$, the $[CuO_6]$ octahedra are connected to each other one dimensionally parallel to the a axis by sharing O(2)–O(2) edges, such that the elongated octahedral axis ordered in the same direction parallel to the c axis, or perpendicular to the $[CuO_{4/2}]_\infty$ plane, which is different from the ordering in the halides (see Fig. 8).

The difference in ordering between the oxides and halides is also found for two dimensional cooperative ordering systems. Halides and oxides with a formula A_2MX_4 adapt the K_2NiF_4 structure, where the M ions ordered two dimensionally (see Table III). Many studies of halides with the K_2NiF_4 structure have revealed an antiferrodistortive ordering of elongated octahedra; the elongated axis ordered in the $[MX_{4/2}]_\infty$ plane. In the oxide La_2CuO_4, on the other hand, ferrodistortive ordering is observed; the octahedral elongated axis ordered perpendicular to the two dimensional $[MO_{4/2}]_\infty$ plane. The cooperative Jahn–Teller ordering in oxides and halides with the edge sharing octahedra is therefore summarized as follows: (i) for halides, the elongated axis ordered in the $[MX_{4/2}]_\infty$ plane either in antiferrodistortive way (two dimensional system) or in ferrodistortive way (one dimensional system); (ii) for oxides, the elongated axis ordered perpendicular to the $[MX_{4/2}]_\infty$ plane in ferrodistortive way for both one and two dimensional systems.

Conclusions

The following results have been obtained in the present study.

(i) The Jahn–Teller distortion in the

$[CuO_6]$ octahedra decreases with the increase in the non-Jahn–Teller Cu^{3+} ions for the low-temperature $Li_{1-x}CuVO_4$ phase.

(ii) The phase transition from the low-temperature to the high-temperature modification is an order–disorder type concerned with the distribution of vacancies and cations on the octahedral sites.

(iii) The high-temperature $Li_{1-x}CuVO_4$ phase has a more random cationic arrangement, which causes a larger Jahn–Teller distortion of the $[CuO_6]$ octahedra.

(iv) One and two dimensional cooperative Jahn–Teller ordering in oxides and halides with edge sharing octahedra is summarized as follows: the elongated axis ordered parallel to the $[MX_{4/2}]_\infty$ plane in the halides, and the elongated axis ordered perpendicular to the $[MX_{4/2}]_\infty$ plane in the oxides.

Acknowledgments

We thank Dr. F. Izumi of NIRIM for providing a computer program RIETAN. All computations for structure determination were carried out at the Mie University Information Processing Center.

References

1. P. J. Wojtowicz, *Phys. Rev.* **116,** 32 (1960).
2. J. D. Dunitz and L. E. Orgel, *J. Phys. Chem. Solids* **3,** 20 (1957).
3. R. Englman and B. Halperin, *Phys. Rev. B* **2,** 75 (1970).
4. D. Babel and A. Tressaud, *in* "Inorganic Solid Fluorides" (P. Hagenmuller, Ed.), p. 156, Academic Press, New York (1985).
5. P. Nunez, J. Darriet, P. Bukovec, A. Tressaud, and P. Hagenmuller, *Mater. Res. Bull.* **22,** 661 (1987).
6. D. Babel, *Z. Anorg. Allg. Chem.* **336,** 200 (1965).
7. R. Kanno, Y. Takeda, K. Murata, and O. Yamamoto, *Solid State Ionics* **39,** 233 (1990).
8. W. J. Crama, *J. Solid State Chem.* **39,** 168 (1981).
9. W. J. Crama, *Acta Crystallogr., Sect. B:* **37,** 2133 (1981).
10. W. J. Crama, M.Bakker, G. C. Verschoor, and W. J. Maaskant, *Acta Crystallogr., Sect. B:* **35,** 1875 (1979).
11. W. J. Crama, W. J. A. Maaskant, and G. C. Verschoor, *Acta Crystallogr., Sect. B:* **34,**1973 (1978).
12. H. W. Zandbergen and D. J. W. Ijdo, *J. Solid State Chem.* **38,** 199 (1981).
13. R. Kanno, Y. Takeda, A. Matsumoto, O. Yamamoto, R. Suyama, and S. Kume, *J. Solid State Chem.* **75,** 41 (1988).
14. J.-C. Joubert, J.-C. Grenier, and A. Durif, *C.R. Acad. Sci. Paris* **260,** 2472 (1965).
15. A. Durif, J.-C. Grenier, J.-C. Joubert and T.-Q. Duc, *Bull. Soc. Fr. Mineral. Cristallogr.* **89,** 407 (1966).
16. F. Izumi, *J. Miner. Soc. Jpn.* **17,** 37 (1985) [In Japanese].
17. D. Reinen and C. Friebel, "Structure Bonding," Vol. 37, p. 7, Springer-Verlag, Berlin/New York (1979).
18. M. T. Hutchings, M. J. Fair, P. Day, and P. J. Walker, *J. Phys. C: Solid State Phys.* **9,** 455 (1976).
19. K. Le Dang, P. Veillet, and P. J. Walker, *J. Phys. C: Solid State Phys.* **10,** 4593 (1977).
20. R. Haegele and D. Babel, *Z. Anorg. Allg. Chem.* **409,** 11 (1974).
21. E. Hardtweck and D. Babel, *Z. Anorg. Allg. Chem.* **474,** 113 (1981).
22. M. Hidaka and P. J. Walker, *Solid State Commun.* **31,** 383 (1979).
23. J. M. Longo and R. M. Raccah, *J. Solid State Chem.* **6,** 526, (1973).
24. Von B. Grande, Hk. Muller-Buschbaum and M. Schweizer, *Z. Anorg. Allg. Chem.* **428,** 120 (1977).
25. W. Massa and M. Steiner, *J. Solid State Chem.* **32,** 137 (1980).
26. R. Kanno, Y. Takeda, A. Takahashi, O. Yamamoto, R. Suyama, and S. Kume, *J. Solid State Chem.* **71,** 196 (1987).
27. R. Kanno, Y. Takeda, A. Takahashi, O. Yamamoto, R. Suyama, and S. Kume, *J. Solid State Chem.* **72,** 363 (1987).